Dynamics and spectral properties of subduction earthquakes

R. Madariaga

Laboratoire de Geologie, CNRS-ENS, PSL University - Paris, France
Departamento de Geofisica, Universidad de Chile - Santiago, Chile

Summary. — We have studied the spectra of several large earthquakes in the Chilean subduction zone using both accelerograms and CNSS instruments. For the two events studied here, the Iquique M_{w} 8.1 earthquake of 24 April 2014 and the M_{w} 6.9 Valparaiso earthquake of 24 April 2017 we observe similar features. For these earthquakes the velocity records at low frequencies obtained by integrating accelerograms agree quite well with the ground velocity derived from GNSS records at the same sites. These observations show that at low frequencies the ground spectra differ quite significantly from the usual Aki-Brune spectrum used in studies of the far-field spectral properties of earthquakes. The most important difference is that at short distances the near-field term of the source dominates the spectra at low frequencies. The near-field term in seismic radiation is proportional to the moment time function of the source which is very different from the moment rate function that controls farfield. The ground velocity spectrum is flat at low frequencies and proportional to the static displacement produced by the earthquke at the observation site. The displacement spectrum on the other hand has a low-frequency asympote proportional to omega -1 instead of the usual flat spectrum predicted by the Aki-Brune model. More theoretical work is needed to identify the region where the near-field spectrum dominates.

1. – Introduction

Most studies of seismic radiation assume that the Fourier spectrum of displacement follows the omega-squared spectrum proposed by Aki and Brune [1, 11]. This is often true in the far field although many deviations from the simple omega-squared model are frequently reported (see, *e.g.* [3, 4]). In the near field it is expected that the spectrum deviates from the simple Aki-Brune model. Among other properties of seismic radiation the near-field spectrum must be compatible with the finite near-field displacement observed by dynamic GPS and the strong motion recordings observed at shorter distances from the source. Here we review a number of observations made in Chile where several large earthquakes have been recorded by both accelerometers and GNSS (Global Navigation Satellite System) instruments. We show that in the near field the seismic spectra are often very different from the Aki-Brune model.

In the last 15 years a number of large subduction earthquakes in North and Central Chile have been very well observed thanks to new observational data obtained by a number of new instruments deployed in the country. The series of events started with the 2005 Tarapaca [35] earthquake of 2005, it was followed by the M_{w} 7.7 Tocopilla earthquake [36] most important event was the M_{w} 8.8 Maule earthquake of 27 February 2010, followed in 2014 by the M_{w} 8.2 Iquique (sometimes called Pisagua) earthquake, the 15 September 2015 Illapel earthquake of M_{w} 8.4 and a series of events of magnitudes between 6 and 8 that provide additional insight into the radiation produced by earthquakes generated by the subduction process in Chile.

In a recent publication by [31] the spectra of the Iquique earthquake was discussed in some detail from the simultaneous observation of ground motion recorded by both accelerometers and GNSS data (see also [5]). They showed that the ground velocity spectrum is flat at low frequencies and that its amplitude is proportional to ground
1 displacement observed by collocated GPS stations. This is in contrast with predictions by Aki-Brune that in the far field the velocity spectrum should increase at low frequencies as ω used in most studies of earthquake spectra [34, 3, 37, 4, 14]. The first observations made in Chile of deviations of the ground motion spectrum from the classical Brune model were made by [24] following the Tocopilla earthquake of November 2017. Although the data was sparse they showed that ground displacement spectra was very different from that of small aftershocks and that it had an omega -1 asymptote at low frequencies. This observation together with others made in for the M_{w} 8.8 Maule earthquake of 27 February 2010, showed that the near-field terms in seismic radiation significantly affects the ground motion spectrum and that the usual assumption that Brune spectrum properly describes the ground motion properties needs to be carefully revised. Of course the effects of the near-field terms are limited to the lower frequency range, but under many circumstances the effect may be much broader than what is usually assumed.

In this notes I will first review the recent observations of ground motion made simultaneously by accelerographs and GNSS instruments in Northern Chile during the Iquique earthquake of 2014 so as to set some broad properties of ground motion, specially ground velocity. Then we will look at a smaller event of magnitude M_{w} 7.9 that occurred near

Valparaiso on 24 April 2017. This event was very well recorded by the new National Seismological Service of the University of Chile (CSN) although only a couple of GPS stations could be used to determine the very low-fequency properties of ground displacement. We will provide a short introduction to ground motion properties derived from the usual Green function in an infinite medium and then provide some discussion about the consequences of these new observations.

2. – Observations

Northern Chile is an active seismic zone that is sometimes considered to be an active seismic gap by many authors [29, 31]. Since 2005 a large set of multi-parameter stations were deployed by the Integrated Plate Boundary Observatory Chile (IPOC), a multi-component network deployed by German, French and Chilean researchers starting from 2006. After 2013 a new network of multi-parameter instruments was deployed by CSN (Centro Sismologico Nacional of the University of Chile). Since then, northern Chile earthquakes have been well recorded by GNSS, broad band and strong motion stations mostly located on hard rock sites [27, 28, 5]. The first mayor earthquake that occurred after the installation of IPOC was the M_w 7.7 Tocopilla earthquake of 2007 [13, 36, 16]. [24] studied the spectral characteristics of this event and its aftershocks. They found that aftershocks had a typical omega-squared Fourier displacement spectrum [1, 11, 30]. The main-shock, on the other hand, was very different since its displacement spectrum diverged at low frequencies, increasing like omega to the power -1. They proposed that this behavior could be due to the presence of near-field waves, but that it could also be due to the complexity of this double event. The lack of near-field GNSS instruments did not permit us to resolve the low-frequency properties of the displacement spectrum in order to distinguish between these two hypotheses.

The large 2010 M_w 8.8, Maule mega-thrust earthquake produced excellent continuous GNSS records that were used by [47] as seismograms to model the rupture process of the event. Unfortunately no digital good-quality accelerometers were located close to the epicenter of the Maule 2010 earthquake [38]. After this event the Centro Sismologico National (CSN) of the University of Chile was created and deployed a large network of broad-band, accelerometers and GNSS stations [6, 27, 28, 5]. These stations have recorded several large earthquakes including the M_w 8.2 Iquique event of 1 April 2014, the M_w 8.3 Illapel earthquake of 15 September 2015 and the M_w 7.6 Chiloé earthquake of 25 December 2016. These events provide excellent recordings that have been largely used to model the events and to study their principal characteristics (*e.g.* [39, 44, 18, 23, 32, 49, 41, 34, 25]). These studies have been centered on the slip distribution, tsunami effects, nucleation process and their relation with slow-slip events, but did not mention the spectral properties of strong-motion records in the near field. Here we examine the general properties of these accelerograms. We use the records written by the Iquique earthquake of 1 April 2014 and the Valparaiso earthquake of 24 April 2017 because these events have a large number of colocated GNNS and strong-motion records on hard-rock 2
sites [28, 27, 5]. Our goal is to understand the basic features of seismic spectra, the

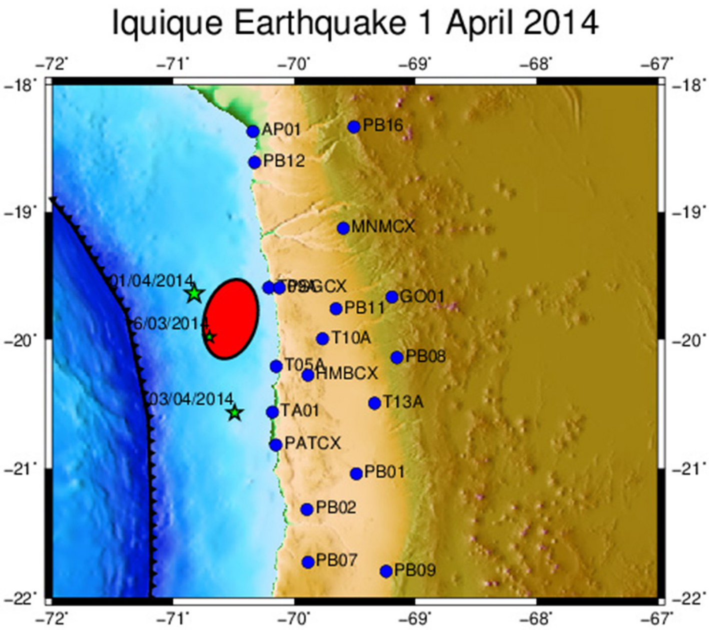

Fig. 1. – Northern Chile area hit by the $M_\mathrm{w} = 8.1$ Iquique earthquake of 1 April 2014. The rupture area of the main event is outlined by the red ellipse (from [39]). White stars show the epicenters of the main shock as well as its main aftershock of 3 April 2014 and the 16 March 2014 foreshock. The events are situated between the trench and the Chilean coast line along the plate interface. The main stations used in the present study are shown with blue circles.

relative role of low and high frequencies of the spectrum and their relation with the seismic moment and seismic moment rate histories.

In the following we use the ground motion records obtained during the Iquique earthquake of 1 April 2014 in Northern Chile. This event was very well recorded by stations from the IPOC network and by several accelerometers of new network deployed by the CSN. The 2014 event was a complex event that had a small immediate precursor and a massive slip located between the foreshock and the mainland (see, *e.g.* [39, 15]). As shown in fig. 1, more than 50 records are available for this event, of which many collo-
3 cated GNSS and accelerograms could be used. We will illustrate data processing using these recordings.

Accelerograms are difficult to integrate to displacement as discussed by [8] who proposed a method to integrate them taking into account changes in the average ground velocity before and after the event. Variations of this technique have been proposed by other authors [8, 20, 48, 9, 12]. Using time domain integration of accelerograms we verified that we could fit the low-frequency features observed in the GNSS records. Several examples of the fit between GNSS recordings and integrated accelerograms in Chile were recently published by [5]. The accelerograms studied here are relatively weak since none of them has a peak ground acceleration (PGA) greater than the 20% of g.

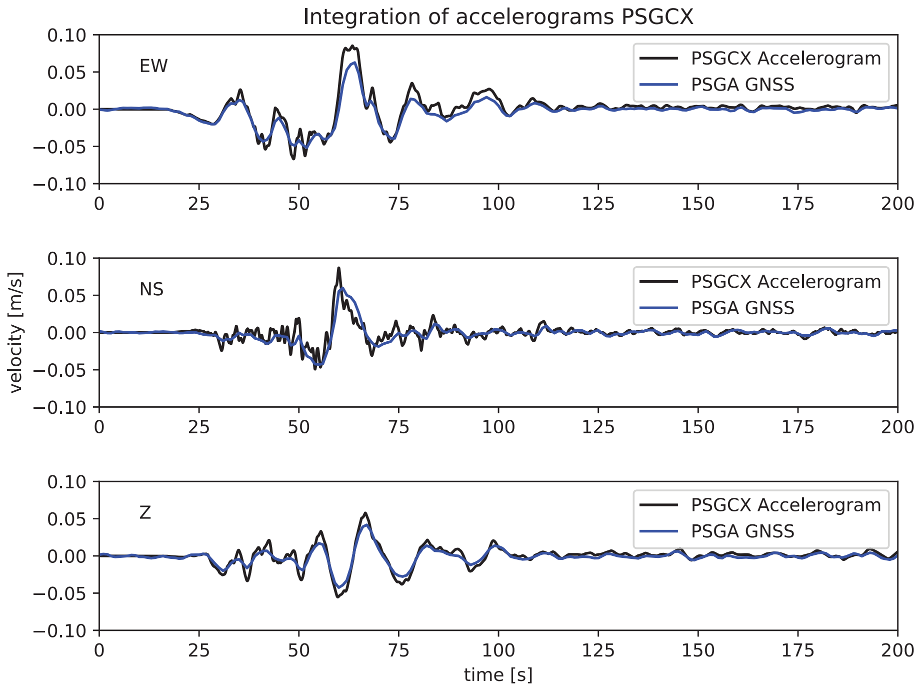

Fig. 2. – Ground velocity at the Pisagua stations computed from GNSS records (PSGA) and co-located integrated accelerogram (PSGCX). The velocity records computed from accelerograms have been low-pass filtered at 0.5 Hz in order to enhance the similarity between GNSS and ground velocity records in their common band pass.

Digital displacement records whether obtained from GNSS records or by integration of accelerograms cannot be used directly to compute displacement spectra because the finite displacement jumps at the end of the record. The reason is that the finite discrete Fourier transform used to compute the spectra records assumes that the time series is periodic with a period equal to the duration of the record. Thus the Fourier transform sees a jump in displacement at the end of the record that contaminates the computed spectrum at all frequencies. The Fourier transform of such a jump is simply the static displacement divided by frequency. All the other spectral information contained in the accelerogram is hidden by this jump. Many techniques have been proposed in the literature to remove this effect of the finite time window. Some of them consist in using a window to multiply the time signal, but these windows contaminate the low-frequency contents.

We propose a simple method to compute the displacement spectrum that uses a property of the velocity time series. The accelerograms integrated once to determine the ground velocity have been shown to be very well fit at low frequencies by the ground velocity derived from GNSS signals (*e.g.* [7,48,5]). Figure 2 shows the three components 4
of the ground velocity integrated from accelerograms at the PSGCX station, and the velocities derived from the nearby PSGA GNSS recordings. The instrument response

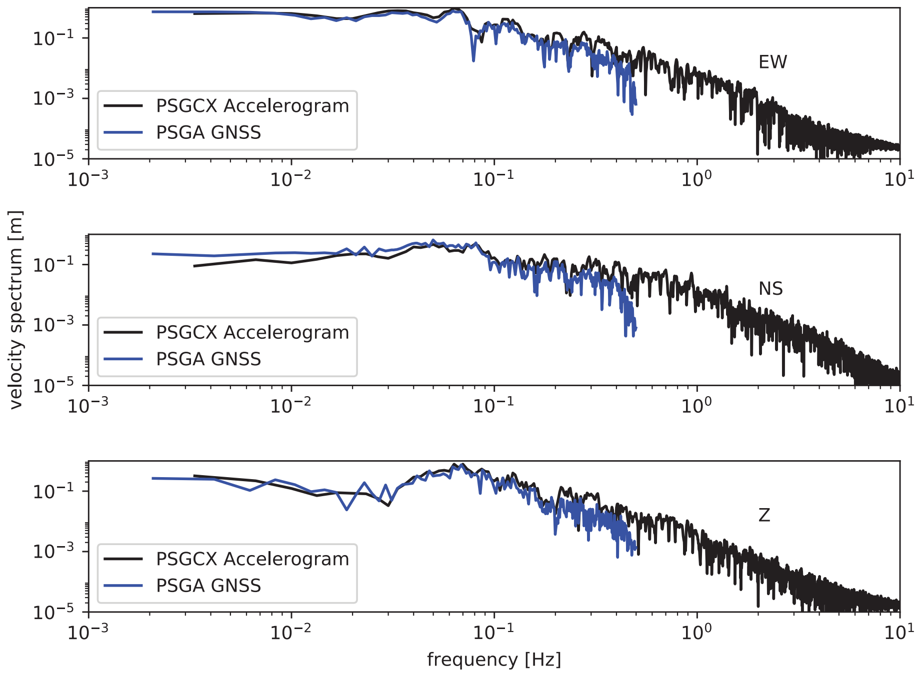

Fig. 3. – Spectra of the ground velocity computed from PSGA GNSS station and the PSGCX accelerogram. The corresponding time domain signals are shown in fig. 2. We observe that at low frequencies the accelerogram and GNSS instrument share an almost identical spectrum in spite of the different noise levels in these two types of instrument. All three components have almost flat spectra at low frequencies whose level is the co-seismic displacement at this site.

of the accelerograms was removed, and the records were low-pass filtered with a causal Butterworth filter of order 2 and corner frequency 0.5 Hz. The coincidence between the records is excellent. This representation is better than comparisons between displacement records to show that the frequency content of the two records is the same in the frequency range where they both coincide (conservatively estimated as above 0.15 Hz).

In fig. 3 we show the Fourier spectra of the velocity traces at stations PGA and PSGCX plotted in fig. 2. Since velocity returns to zero at the end of traces, except for seismic noise, we can compute the velocity spectrum without the problems of the finite displacement at the end of the time window discussed earlier. The spectra computed using regular FFT routines display a common property of ground velocity for large subduction earthquakes in Chile. The spectral trend is flat at low frequencies in contrast to predictions of far-field velocity radiation for finite sources [11,30] that it should linearly increase with fequency at low frequencies. A more detailed explanation will be provided in next section, but it is relatively easy to understand. At close distances from the source the near-field terms of the Green function dominate the radiated spectrum. The near field is dominated by the moment time function, not the moment rate, so that at close distances the velocity spectrum at low frequencies resembles that of the integral of the far field source-time function.

3. – Theory

Computing the full field radiated by a finite seismic source embedded in a heterogeneous earth model is difficult and can only be done numerically for certain models of structure. For example, for layered media it is possible to compute the full field using spectral integration methods like Axitra [10]. Because we want to gain intuition on the properties of the field we will study here the simplest situation of a point double couple source embedded in a homogeneous elastic space.

3˙1. *Near field from a point source in an infinite medium.* – The Green's function for a point moment tensor source inside an infinite elastic medium can be written [2] as

$$u(r,t) = \frac{1}{4\pi\rho}\frac{1}{r^4}A^N \int_{r/\alpha}^{r/\beta} \tau M_0(t-\tau)\mathrm{d}\tau + \frac{1}{4\pi\rho\alpha^2}\frac{1}{r^2}A^{IP}M_0(t-r/\alpha) + \frac{1}{4\pi\rho\beta^2}\frac{1}{r^2}A^{IS}M_0(t-r/\beta) + \frac{1}{4\pi\rho\alpha^3}\frac{1}{r}A^{FP}\dot{M}_0(t-r/\alpha) + \frac{1}{4\pi\rho\beta^3}\frac{1}{r}A^{FS}\dot{M}_0(t-r/\beta). \tag{1}$$

This expression is usually interpreted as if the near field contained two terms: one called the near field inversely proportional to r^{-4}, and the other called intermediate field that decays like r^{-2}. Actually the first term decays in fact as r^{-2} because the integral on the first line of (1) grows with distance as r^2. In this expression the coefficients $A^N, A^{IP}, A^{IS}, A^{FP,}$ and A^{FS} are the radiation patterns. $M_0(t)$ is the moment tensor time history and $\dot{M}_0(t)$ is the moment rate time function. Thus the near field is proportional to moment, while the far field is proportional to moment rate. The time domain expression (1) is difficult to separate into P and S waves because the near-field term (the integral) can be only be split into two diverging integrals that cancel each other for times greater than the arrival time of the S-wave.

For this reason we prefer to use the frequency domain expression. We use the following definition of the Fourier transform:

$$\tilde{f}(\omega) = \int_{-\infty}^{\infty} f(t)e^{-i\omega t}, \tag{2}$$

which has different sign in the exponential from that adopted by [2].

The time domain Green function (1) can be transformed into

$$
u(\tilde{r},\omega) = \frac{M_0(\omega)}{r^2}\left[\frac{1}{4\pi\rho\alpha^2}F^{INP}(\omega r/\alpha)e^{-i\omega r/\alpha} + \frac{1}{4\pi\rho\beta^2}F^{INS}(\omega r/\beta)e^{-i\omega r/\beta}\right]
+\frac{\dot{M}_0(\omega)}{r}\left[\frac{1}{4\pi\rho\alpha^3}A^{FP}(\omega r/\alpha)e^{-i\omega r/\alpha} + \frac{1}{4\pi\rho\beta^3}A^{FS}(\omega r/\beta)e^{-i\omega r/\beta}\right], \tag{3}
$$

where the coefficients F^{INP}, and F^{INS} are

$$
F^{NP}(\omega r/\alpha) = A^N\frac{\alpha^2}{\omega^2 r^2}\left(\frac{i\omega r}{\alpha}+1\right) + A^{IP}
$$

and

$$
F^{NS}(\omega r/\beta) = -A^N\frac{\beta^2}{\omega^2 r^2}\left(\frac{i\omega r}{\beta}+1\right) + A^{IS},
$$

these are self-similar functions of the non-dimensional frequency times distance divided by elastic wave speed. The near and intermediate field radiation patterns A^N, A^{IP}, A^{IS} are defined in [2].

The frequency domain Green function clearly states that there are two types of terms in the radiated elastic field: Near-field terms that are proportional to the moment time function $M_0(\omega)$ and decay like r^{-2}; and far-field terms that are proportional to the moment rate $\dot{M}_0(\omega)$ and decay like r^{-1}. What is not clear from these expressions is at which distance range the near and far field dominate. There is a clear transition for each type of wave depending on the non-dimensional term $\omega r/\alpha$ for P-waves and $\omega r/\beta$ for S-waves. The near-field terms in (3) interfere strongly so that at large distances the time difference between the arrival time of P and S waves plays an important role.

For the moment we study separately the P and S waves in order to gain some understanding of the relative role of the near and far field terms.

3·2. *A simplified model.* – Dealing with the whole expression in (1) or (3) is not very practical to understand the relative roles of the near- and far-field terms in the Green function. We adopt an approximation in which we neglect the frequency-dependent term in the coefficients F. This approximation was used by [46] in the study of the near field of the deep Peruvian earthquake of 1994 observed by stations located above the source. Here we approximate the S-wave by the following expression in the frequency domain:

$$
u^S(r,\omega) = \frac{C^{NF}}{r^2}M_0(\omega) + \frac{C^{FF}}{r}\dot{M}_0(\omega), \tag{4}
$$

where C^{NF} represents the near-field radiation pattern and normalization; and C^{FF} is the normalized far-field radiation pattern. This expression shows that the spectrum contains terms proportional to the moment and moment rate spectra. In the far field only the last terms are usually considered. The limit at low frequencies of this expression tends to

$$\lim_{\omega \dashrightarrow 0} u^S(r,\omega) = C^{NF} M_0(\omega) = C^{NF} \frac{M_0}{i\omega} \,. \tag{5}$$

Thus the near-field spectrum is dominated by the seismic moment divided by $i\omega$. so that the low frequency displacement spectrum is dominated by the omega -1 asymptote.

An even more interesting relationship is that the Fourier spectrum of the ground velocity can be derived as

$$\lim_{\omega \dashrightarrow 0} \dot{u}^S(r,\omega) = C^{NF} M_o = u(r,0). \tag{6}$$

Thus the Fourier velocity spectrum of the ground velocity tends to be flat at low frequencies and its amplitude is a measure of the static ground displacement. Expression (6) was derived here for the approximation (4), but it is a compltely general property of ground velocity spectra, whether the source is in an infinite or a heterogeneous medium. This expression should facilitate the computation of the static ground displacement once ground velocity has been computed without the need of the inaccurate double integration of the accelerograms.

Let us now compute the spectrum expected at stations where the near field is important. For that purpose we adopt Brune's far-field radiation model. The source time function for this model is

$$\dot{M}_0(t) = M_0 \omega_0^2 t\, e^{-\omega_0 t} H(t), \tag{7}$$

where ω_0 is the corner frequency of the signal. Its spectrum is well known:

$$\dot{M}_0(\omega) = M_0 \frac{\omega_0^2}{(\omega_0 + i\omega)^2} \,. \tag{8}$$

At low frequencies the moment rate spectrum tends to M_0 the static moment of the source. Any other source time funstion may be used but in most applications brune's model (4) is most often used.

The moment time history for this signal is rather complicated to write but very simple:

$$M_0(t) = M_0 \left[1 - (1 + \omega_0 t)\, e^{-\omega_0 t}\right] H(t). \tag{9}$$

The spectrum of the Moment time function is just (5) divided by $i\omega$.

In fig. 4 we show the expected near-field record of diplacement that contains both near and far-field terms. The corner frequency has been chosen as $f_0 = 0.637$ and the corresponding circular frequency is $\omega_0 = 2\pi f_0 \sim 4$ and a ratio $C = C^{NF}/(rC^{FF}) = 1$. This produces a near-field signal that is very similar to those observed by dynamic GPS records, or doubly integrated from accelerograms. In fig. 5 we plot the near-field spectrum

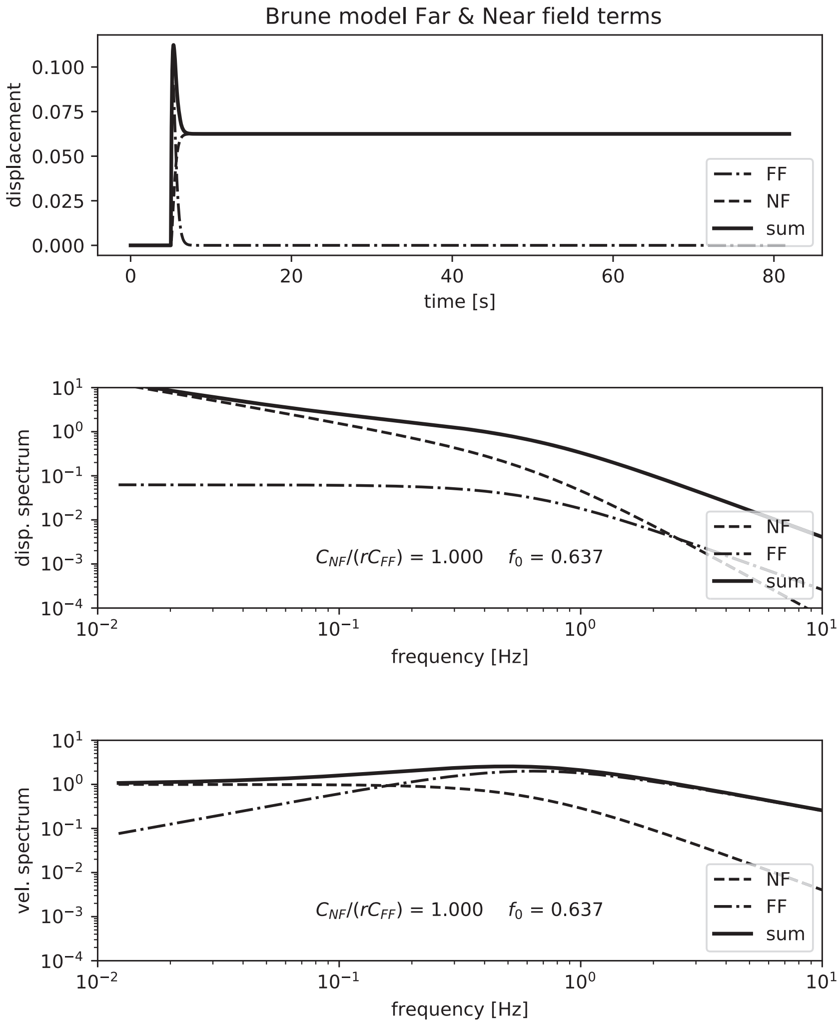

Fig. 4. – Near-field record and spectrum when the near-field term is large compared to the far field source time function. Here the coefficient in (4) is $C^{NF}/(r * C^{FF}) = 1$.

and displacement time signal for the same corner frequency and a ratio $C = 0.25$. We observe that the near field is now small so that the peak of the far-field velocity spectrum starts to emerge. The displacement spectrum, on the other hand, starts to be similar to the far-field spectrum of the Brune model.

4. – The 1 April 2014 Iquique earthquake

On 1 April 2014 a magnitude M_{w} 8.2 hit the Northern Chile region of Tarapacá near the cities of Iquique and Pisagua. Two days later the largest aftershock with magnitude

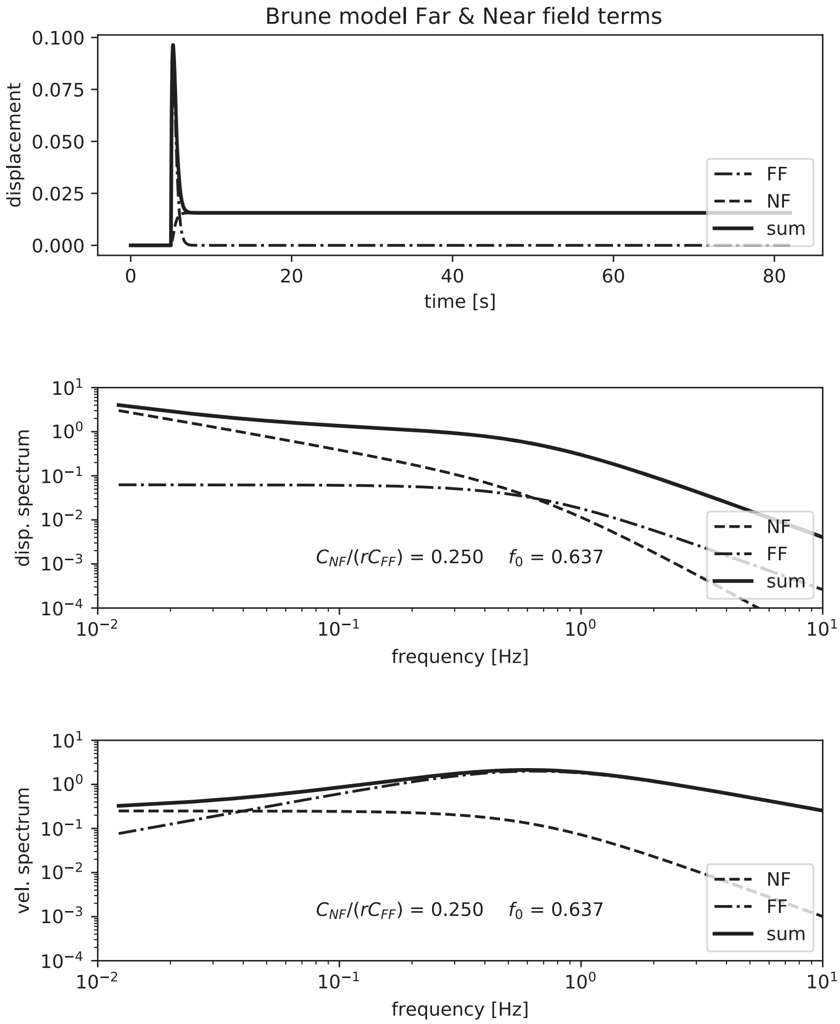

Fig. 5. – Near-field record and spectrum when the near-field term is large compared to the far-field source time function. Here the coefficient in (4) is $C/r * C^{FF} = 0.25$.

M_{w} 7.7 occurred (see fig. 1) [39,44,23,15]. This event has been studied by many authors, specially because it was preceded by a long series of precursory shocks that began several years before 2014 and culminated in an intense, but intermittent series of fore-shocks that started in July 2013 [26]. A slow-slip event was observed before the main shock that has been carefully documented [39, 22, 45]. The main event was studied by a number of researchers using a combination of far- and near-field data that were reviewed by [15].

In the previous section we studied the recordings at the PSGCX collocated with the 5
PSGA GNSS instrument in Northern Chile near the town of Pisagua. This is the closest station to the earthquake epicenter and as shown in fig. 1. The velocity records de-

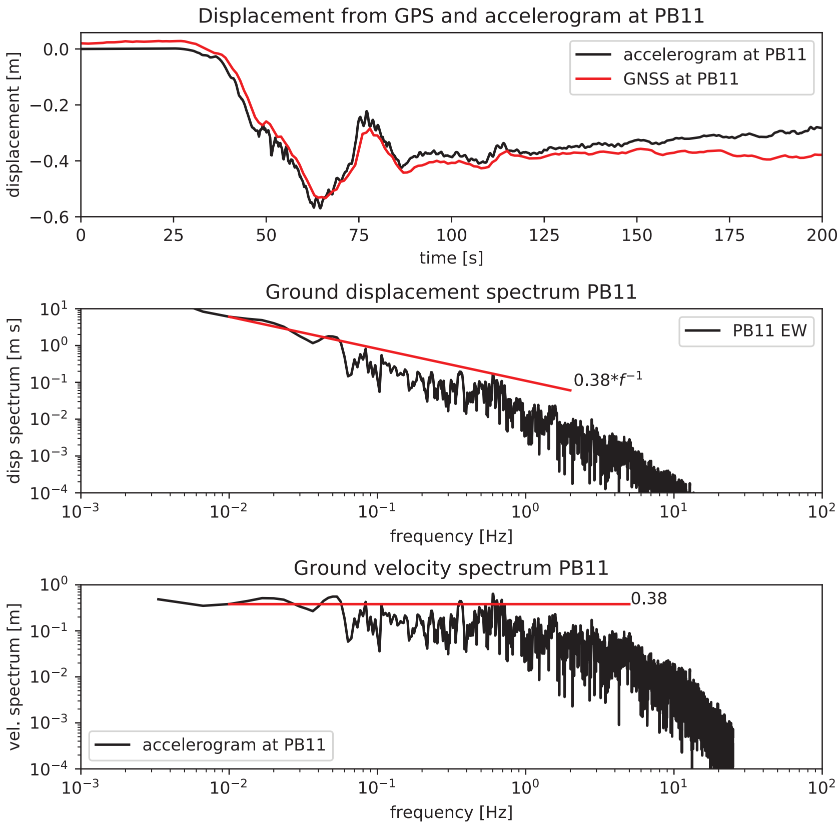

Fig. 6. – EW component of displacement integrated from the accelerogram of the PB11 station located 119 km from the epicenter of the 1 April 2014 Iquique earthquake of M_{w} 8.1. At the top the displacement waveform computed by integrating the accelerogram is compared with the displacement recorded by the co-located GNSS station. At the bottom, the displacement and velocity spectra computed from the accelerogram. Thei amplitude of the flat portion of the velocity spectrum agrees very well with the displacement jump of 0.38 m observed in the GNSS record.

rived from GNSS instruments and accelerometers are essentially identical in the common frequency band of the two records (figs. 2 and 3). At this short distance the seismic moment-dependent terms in the Green function, first term in (3), dominate the spectrum. As shown in fig. 1 more than 20 stations recorded this event in the near field. Of these, we chose the records furnished by the PB11 station which is situated some 60 km inland from Pisagua and 119 km from the immediate fore-shock of the earthquake. Figure 5 shows the EW component of displacement at this station using the Boore [8] procedure discussed earlier. Superimposed on the seismic displacement trace we plot the ground displacement recorded by GNSS instrument at the PB11 IPOC multi-parametric station. The traces for both the integrated accelerogram and the geodetic data are very

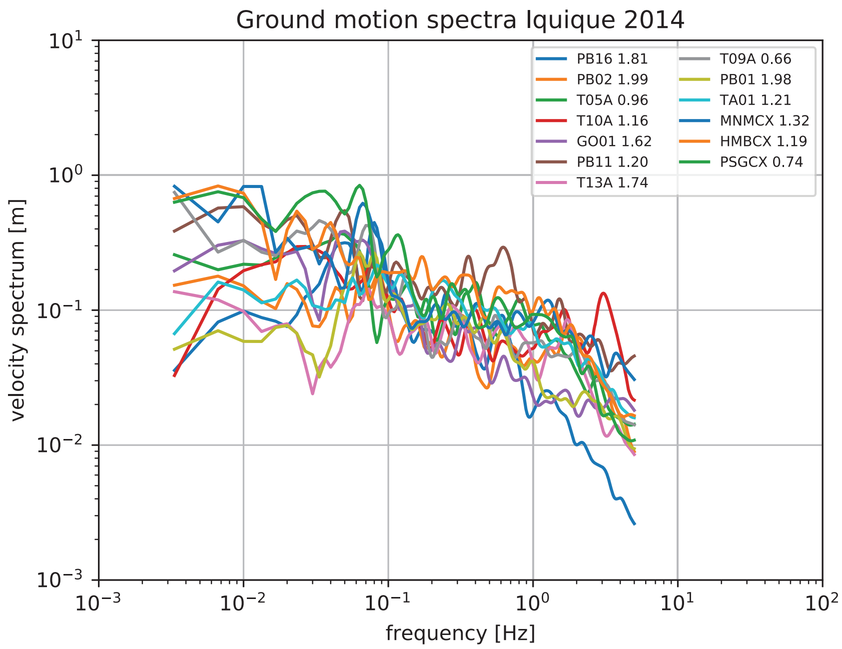

Fig. 7. – Stack of velocity spectra for 14 accelerograms that recorded the 1 April 2014 Iquique earthquake. These spectra were computed by standard Fourier transform of the ground velcoity records obtained by direct integration of accelerograms. Accelerograms were corrected by the instrument response and a removal of the mean acceleration.

similar and have a large static component. It is obvious that in this station the field is dominated by the moment time-function. In the two bottom panels of fig. 8 we show the 6 ground displacement and velocity spectra computed from the accelerogram spectrum by double Fourier integration (division by omega -2). The displacement spectrum shows the characteristic omega -1 decay expected at low frequency. The velocity spectrum at the bottom has the typical flat spectrum observed for many large subduction earthquakes in Chile. The level of the flat part of the velocity spectrum is very close to the static displacement observed in the GNSS instrument trace (GPS) at the top of fig. 8, 7 confirming relation (6) derived earlier.

In fig. 6 we show a stack of the ground velocity spectra computed for the EW com- 8 ponent of 14 accelerograms that recorded the Iquique main shock at distances varying from 80 to 250 km. Although amplitudes are quite variable the shape of the spectra are very similar with a flat low frequency asymptote, a peak near 0.08 Hz (12.5 s) and an omega -1 decay in the frequency range from 1 to 10 Hz.

5. – The 24 April 2017 Valparaiso earthquake

An important subduction earthquake occurred near Valparaiso in the center of Chile on 24 April 2017. This event of M_{w} 6.9 was preceded by a strong fore-shock activity

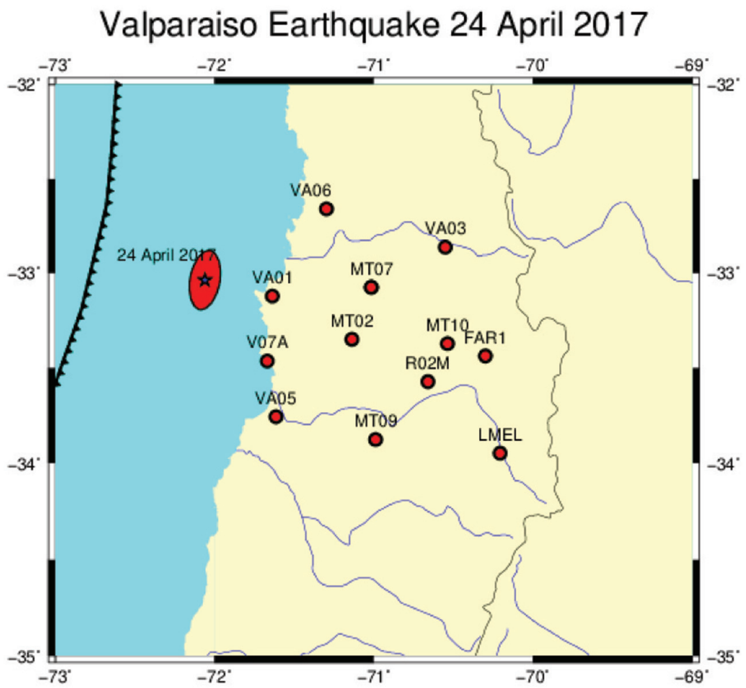

Fig. 8. – Valparaiso earthquake of 24 April 2017. The epicenter of this $M_w = 6.9$ earthquake is indicated by the blue star. The red circles denote the accelerometers used in the present work. The red ellipse over the hypocenter is the main rupture area as determined by dynamic inversion by [41].

that included large events on 22 April 2004 and was preceded by an immediate slow-slip event. The earthquake itself occurred very close to the site of the large M_w 8.0 earthquake in Valparaiso of 3 March 1995. The Valparaiso event was very well recorded by a number of seismic stations from the CSN network. Due to its relatively moderate size it was only recorded by the GNSS sites located very close to the coast. This event was the object of several studies [41, 43, 18]. The area where the Valparaiso earthquake occurred is particularly interesting because it was the site of one of the largest subduction earthquakes in the history of Chile, the 8 July 1730 earthquake. More recently Valparaiso was hit by several earthquakes of magnitude close to 8: 1821, 1906, 21 July 1971, 3 March 1985 and several others.

In fig. 8 we show the location of the earthquake and the set of accelerograms that recorded the event. There are many more than these of course but we did not used them in our study.

5˙1. *Observations of the Valparaiso earthquake.* – The closest stations to the Valparaiso earthquake were two neighboring stations in Valaparaiso city. these were the VALN high-rate GNSS site and the VA01 accelerometer of the CSN National network. The records

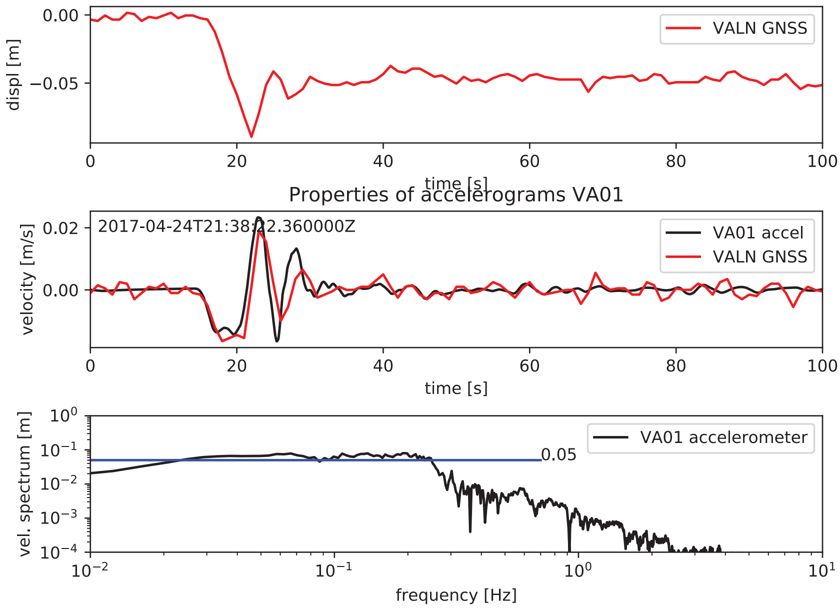

Fig. 9. – Observation of the Valparaiso earthquake of 24 April 2017 at the VALN GNSS station and the neighboring accelerogram at the VA01 CSN site. At the top we show the EW displacement observed by the VALN GPS. The static jump is 0.05 m westwards. The central panel shows the EW ground velocity signal computed from the VA01 acceleorgram and the GNSS record shown in the first panel. The last panel shows the spectrum of ground velocity computed from the accelerogram at VA01. The long plateau of the ground velocity spectrum has an amplitude that is just the static jump observed at the VALN GNSS record.

show all the usual properties discussed in the present work. We observe for instance that the VALN site moved about 5 cm to the West during the earthquake. The second panel in the fig. 9 shows the comparison between the ground velocity obtained from the GNSS record by differentiation and the from the VA01 accelerogram integrated once to velocity. No special processing was applied to the accelerogram except the removal of the instrument response that ony affects high frequencies, and the removal of the mean. Detrending the record would perturb the ground velocity computed by integration at this station. In the bottom panel of fig. 9, we present the ground velocity spectrum at station VA01 computed by classical FFT from the velocity trace integrated from the accelerogram. We observe clearly the flat low-frequency spectrum predicted by the theory discussed in previous sections. We also observe that the level of the velocity spectrum is 0.05 m (5 cm) as observed by the static displacement recorded by the VALN.

As we move away from the coast the GNSS records cannot be used to determine static ground displacement because noise dominates the records. Thus we have to use the accelerometers to try to understand the properties of the near earthquake spectrum. In fig. 10 we show a profile of 5 representative velocity records observed at a subset of

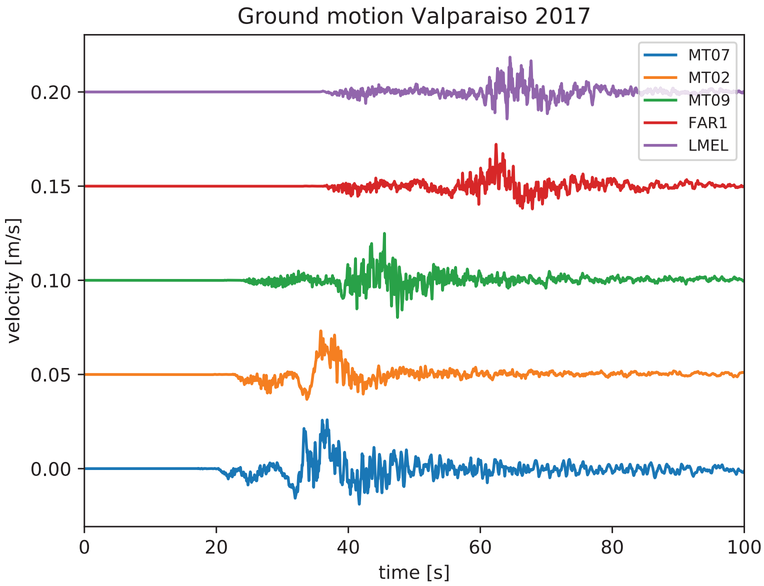

Fig. 10. – Stack of ground velocity records. These velocity signal were integarted from the accelerograms recorded five stations of the central Chile accelerometric network. The traces have been displaced by 0.05 m/s in order to appreciate the propagation of the velocity wavfunctions across the network.

the sites shown in fig. 8. Although the profiles are located inland they were not recorded along a line so that we cannot observe relative propagation of certain P- or S-wave phases. We have many more records but we reduced the number of records to avoid clutter. The figure shows that it is possible to study this event thanks to the velocity records that clearly show the P- and S-wave arrivals as well as a double P- and S-wave waveform. This is related to a small precursor of the 14 April 2017 earthquake that can be identified in some of the accelerograms close to the coast. The precursor occurred roughly by 5 s before the main onset. The double waveform is also observed in the VA01
9 GNSS record shown in fig. 9b. We have not fully explored the records but there is a clear crustal phase between the P- and S-wave in the FAR1 and LMEL records at about 50 s.

Finally in fig. 11 we show a stack of the spectra of the ground velocity section shown in fig. 10. The records have not been corrected by any distance move-out, these are the raw spectra. The spectra have been smoothed at high frequencies so as to show the main features of the spectra. The similarity between the records is striking. All of them contain a peak near 0.05 to 0.1 Hz (20 to 10 s period) that is clearly related to the duration of the S-wave in the velocity records of fig. 10. For frequencies higher than this characteristic (corner) frequency we observe a decay as omega -1 predicted by the Aki Brune ground velocity spectrum (this is equivalent to the omega -2 decay in displacement). For frequencies lower than the peak in fig. 11 (frequencies below 0.05 Hz) we observe the development of the velocity plateau. This plateau is clearly related to the distance of the stations from the source.

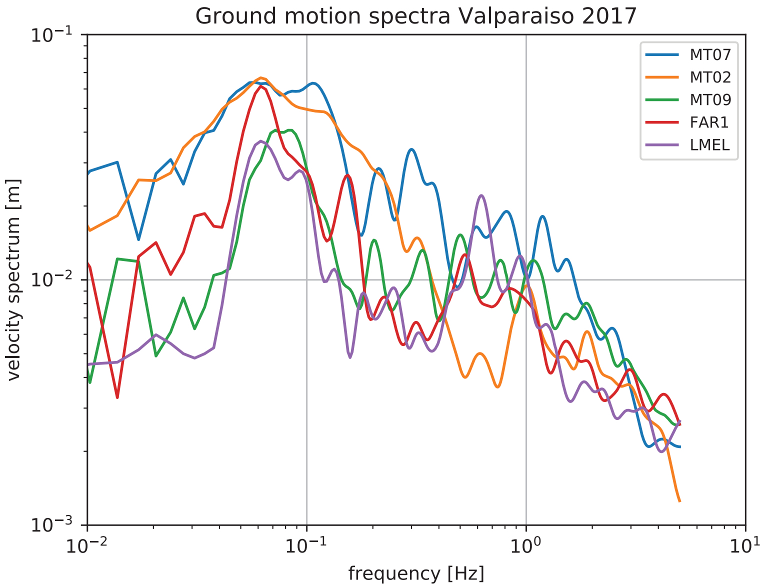

Fig. 11. – Stack of ground velocity spectra observed at the EW components of five accelerometric stations of the Central Chile network of the National seismological Center (CSN).

Finally let us consider the transition to a Brune (far field) like behavior. Station LMEL situated nearly 194 km from the source is sufficiently far although some effect of the near-field terms are still observed in the spectral stack of fig. 11. In fig. 12 we show at the top the EW velocity record at station LMEL obtained by the standard integration of the accelerogram records. The station is sufficiently far from the source of the earthquake because the S-P time (about 20 s) is longer than the duration of the source (about 10 s). The black line is the original EW velocity trace at LMEL, while the red trace is the S-wave windowed by a simple Kaiser window with Beta=6. The two traces coincide well around the S-wave and they have the maximum velocities in the record. In the central panel of fig. 12 we plot the displacement record integrated directly from the first trace, both for the entire record (black) and the windowed S-wave (red). We observe that as expected at far distances from the source the seismic record contains essentially the far field terms, because the near field has become much weaker in this distant stations. In fig. 12 we show exactly that. It is interesting to note however that the velocity spectrum for the window is nearly flat for frequencies higher than 10 Hz, while the full record (black line) increases up to 0.1 Hz. The origin of this difference is the persistence of near-field terms arriving between the P and S wave even at 194 km from the source.

6. – Discussion

It is curious that the observation of near-field terms in the radiation from large earthquakes seems not to have been previously reported. The main reason seems to be that

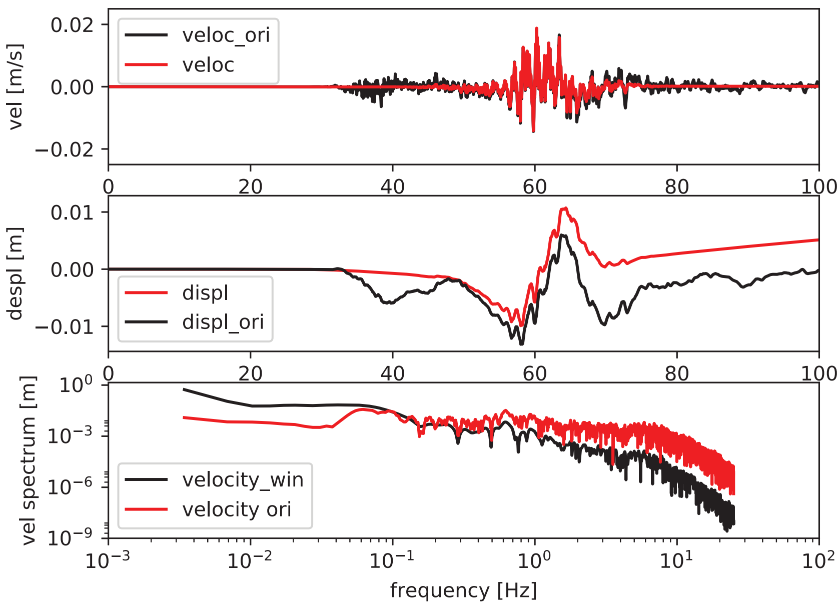

Fig. 12. – Transition to a Brune-like spectral behavior. Station LMEL is the furthest accelerogram available for this event. The top panel shows the ground velocity at MEL integrated from the original accelerogram in black and the windowed record in red. The next panel shows the integrated dispalcement at the same station. Finally, the lower panel shows the velocity spectrum computed by Fourier transform of the top panel.

low frequencies were systematically removed because they are considered inaccurate due to the problem with recovering the static component from near-field accelerograms. This is of course a serious problem that has to be resolved if possible. For the last 20 years, however, low frequency information about seismic source is available from continuous GNSS recordings ([5] and references therein). The simultaneously recording of GNSS and accelerograms can produce a very broad-range version of the ground motion spectrum that can be used for modeling large seismic events without separating the static (GPS) from the dynamic (usually band limited ground displacements). In the present lecture we examine ground velocity spectra. For most earthquakes in Chile, and probably elsewhere, ground velocity integrated from accelerograms can be compared with GNSS records filtered in a common band. These records agree very well, giving confidence that the velocity field has been recorded over a very broad band. We have shown that here for the great 2014 earthquake in Iquique in Northern Chile and for the Valparaiso M_{w} 6.9 earthquake of 24 April 2017. The most important observation made here is that the near-field term contributes significantly to ground motion in a very large region where even if P and S waves are separated, the spectrum computed by classical methods contain large contributions of the so-called omega -1 in displacement, or a large flat plateau in ground velocity spectrum. This plateau has an spectral level roughly equal to the static displacement produced at the observation site by the earthquake. This property has to be verified and tested for many other earthquakes. The main application is determining approximate ground displacements from the Fourier transform of ground velocity. More important perhaps, is that this observation provides a simple way to scale ground velocity spectra that in turn controls the more usual measurements made by engineers and seismologists (PGV and PGA, for instance).

We have purposefully kept the theoretical modeling at its simplest, making an attempt to show the most salient features of seismic radiation in the near field. This feature is that near-field terms are proportional to the moment time function, that is a unipolar function that grows continuously from zero to the static displacement level. This property is largely used in many studies of seismic moment, for instance in the termination of centroid and amplitude of the source time function. The full consequences of this relationship between ground velocity spectrum and static displacement will need further studies because it is independent of the elastic medium in which the waves propagate, but it depends heavily on the distance traveled by the seismic waves and, in particular on the P-S travel time. A careful study of this problem is required.

One of the features that we have observed for the 24 April 2017 Valparaiso earthquake is the detachment of P and S waves at high frequencies at stations located far from the source (more than 150 km). The spectrum of the windowed shear wave and that of the full record are very similar. This indicates that S waves dominate the spectrum and carry all information about the source in the transition region from near field to far field. It would be nice to have a simple expression that defines the boundary between near and far field dominated regions. Unfortunately this is not simple because propagation in the structure between the source and the accelerometers must be properly modelled and taken into account. That will require much further work.

7. – Conclusions

Using collocated GNSS and accelerograms we have found that ground velocity time 10
and spectral signals from these two kinds of instruments coincide largely in their common frequency band, roughly from 0.01 to 1 Hz. We observe that the spectrum of ground motion in the vicinity of large subduction earthquakes is quite different from the classical Aki-Brune far-field spectrum, The reason is that over a large area surrounding the source the near-field terms in the Green's function are large and dominate the spectrum. The most important feature is that the ground velocity spectrum has a long flat spectral plateau with amplitude proportional to the static displacement at the recording site. The properties of this plateau are independent of the medium in which the elastic waves propagate and, we believe, should be further studied for other events.

* * *

This study was supported by FONDECYT contract N° 1170430 and by PRS (Programa Riesgo Sísmico of Universidad de Chile).

REFERENCES

[1] Aki K., *J. Geophys. Res.*, **73** (1967) 5359.
[2] Aki K. and Richards P. G., *Quantitative seismology* (University Science Books, Sausalito) 2002, ISBN 0-935702-96-2.
[3] Allmann B. P. and Shearer P. M., *J. Geophys. Res.*, **114** (2009) B01310.
[4] Archuleta R. J. and Ji C., *Geophys. Res. Lett.*, **43** (2016) 12004.
[5] Baez J. C., Leyton F., Troncoso C., del Campo F., Bevis M., Vigny C., Moreno M., Simons M., Kendrick E., Parra H. and Blume F., *Seismol. Res. Lett.*, **89** (2018) 1546.
[6] Barrientos S. and National Seismological Center Team, *Seismol. Res. Lett.*, **89** (2018) 467.
[7] Bock Y., Melgar D. and Crowell B. W., *Bull. Seismol. Soc. Am.*, **101** (2011) 2904.
[8] Boore D. M., *Bull. Seismol. Soc. Am.*, **91** (2001) 1199.
[9] Boore D. M. and Bommer J. J., *Soil Dyn. Eq. Eng.*, **25** (2005) 93.
[10] Bouchon M., *Bull. Seismol. Soc. Am.*, **71** (1981) 959.
[11] Brune J., *J. Geophys. Res.*, **75** (1970) 4997.
[12] Chao W., Wu Y. and Zhao L., *J. Seismol.*, **14** (2009) 495.
[13] Delouis B., Pardo M., Legrand D. and Monfret T., *Bull. Seismol. Soc. Am.*, **99** (2009) 87.
[14] Denolle M. A. and Shearer P. M., *J. Geophys. Res.*, **121** (2016) 6533.
[15] Duputel Z., Jiang J., Jolivet R., Simons M., Rivera L., Ampuero J. P., Riel B., Owen S. E., Moore A. W., Samsonov S. V. and Ortega Culaciati F., *Geophys. Res. Lett.*, **42** (2015) 7949.
[16] Fuenzalida A., Schurr B., Lancieri M. and Madariaga R., *Geophys. J. Int.*, **194** (2013) 1216.
11 [17] Graizer V., *Seismol. Res. Lett.*, **81** (2010) 635.
[18] Hayes G. P., Herman M. W., Barnhart W. D., Furlong K. P., Riquelme S., Benz H. M., Bergman E., Barrientos S., Earle P. S. and Samsonov S., *Nature*, **512** (2014) 295.
12 [19] Ide S. and Beroza G. C., *Geophys. Res. Lett.*, **28** (2001) 3349.
[20] Iwan W., Moser M. and Peng C., *Bull. Seismol. Soc. Am.*, **75** (1985) 1225.
[21] Jiao W., Wallace T. C., Beck S., Silver P. G. and Zandt G., *Geophy. Res. Lett.*,
13 **22** (1995) 2285.
[22] Kato A. and Nakagawa S., *Geophys. Res. Lett.*, **41** (2014) 5420.
[23] Lay T., Yue H., Brodsky E. E. and An C., *Geophys. Res. Lett.*, **41** (2014) 3818.
[24] Lancieri M., Madariaga R. and Bonilla F., *Geophys. J. Int.*, **188** (2012) 469.
[25] Lange D., Ruiz J., Carrasco S. and Manríquez P., *Geophys. J. Int.*, **213** (2017) 210.
[26] Leon-Rios S., Ruiz S., Maksymowicz A., Leyton F., Fuenzalizada A. and Madariaga R., *J. Seismol.*, **20** (2016) 1059.
[27] Leyton F., Leopold A., Hurtado G., Pasten C., Ruiz S., Montalva G. and Saez E., *Seismol. Res. Lett.*, **89** (2018) 519.
[28] Leyton F., Pasten C., Ruiz S., Idini B. and Rojas F., *Seismol. Res. Lett.*, **89** (2018) 512.
[29] Lomnitz C., *Seismol. Res. Lett.*, **75** (2014) 368.
[30] Madariaga R., *Bull. Seism. Soc. Am.*, **65** (1976) 163.
[31] Madariaga R., Ruiz S., Rivera E., Leyton F. and Baez J. C., *Pure Appl. Geophys.*, (NN) 2018.
[32] Melgar D., Fan W., Riquelme S., Geng J., Liang C., Fuentes M., Vargas G., Allen R. M., Shearer P. M. and Fielding E. J., *Geophys. Res. Lett.*, **43** (2016) 961.

[33] MELGAR D., RIQUELME S., XU X., BAEZ J. C., GENG J. and MORENO M., *Earth Planet. Sci. Lett.*, **474** (2017) 68. 14
[34] OTH A., BINDI D., PAROLAI S. and DI GIACOMO D., *Geophys. Res. Lett.*, **37** (2010) L19304.
[35] PEYRAT S., CAMPOS J., DE CHABALIER J. B., PEREZ A., BONVALOT S., BOUIN M. P., LEGRAND D., NERCESSIAN A., CHARADE O., PATAU G. and CLEVEDE E., *Geophys. Res. lett.*, **33** (2006) 10.1029/2006GL027710.
[36] PEYRAT S., MADARIAGA R., BUFORN E., CAMPOS J., ASCH G. and VILOTTE J. P., *Geophys. J. Int.*, **182** (2010) 1411.
[37] PRIETO G. A., SHEARER P. M., VERNON F. L. and KILB D., *J. Geophys. Res. B*, **109** (2004) NN.
[38] RUIZ S., MADARIAGA R., ASTROZA M., SARAGONI G. R., LANCIERI M., VIGNY C. and CAMPOS J., *Earthquake Spectra*, **28** (2012) S1.
[39] RUIZ S., METOIS M., FUENZALIDA A., RUIZ J., LEYTON F., GRANDIN R., VIGNY C., MADARIAGA R. and CAMPOS. J., *Science*, **345** (2014) 1165.
[40] RUIZ S., KLEIN E., DEL CAMPO F., RIVERA E., POLI P., METOIS M., VIGNY C., BAEZ J. C., VARGAS G., LEYTON F., MADARIAGA R. and FLEITOUT L., *Seismol. Res. Lett.*, **87** (2016) 789. 15
[41] RUIZ S., ADEN-ANTONIOW F., BAEZ J. C., OTAROLA C., POTIN B., DEL CAMPO F., POLI P., FLORES C., SATRIANO C., LEYTON F., MADARIAGA R. and BERNARD P., *Geophys. Res. Lett.*, **44** (2017) NN. 16
[42] RUIZ S. and MADARIAGA R., *Tectonophysics*, **733** (2018) 37. 17
[43] RUIZ J. A., CONTRERAS-REYES E., ORTEGA-CULACIATI F. and MANRÍQUEZ P., *Phys. Earth Plan. Int.*, **279** (2018) 1.
[44] SCHURR B., ASCH G., HAINZL S., BEDFORD J., HOECHNER A., PALO M., WANG R., MORENO M., BARTSCH M., ZHANG Y. and ONCKEN O., *Nature*, **512** (2014) 299.
[45] SOCQUET A., VALDES J. P., JARA J., COTTON F., WALPERSDORF A., COTTE N., SPECHT S., ORTEGA F., CARRIZO D. and NORABUENA E., *Geophys. Res. Lett.*, **44** (2017) 4046.
[46] VIDALE J., GOES S. and RICHARDS P. G., *Geophys. Res. Lett.*, **22** (1995) 1.
[47] VIGNY CH., SOCQUET A., PEYRAT S., RUEGG J.-C., METOIS M., MADARIAGA R. *et al.*, *Science*, **331** (2011) 1417.
[48] WANG G., BOORE D. M., IGEL H. and ZHOU C., *Bull. Seismol. Soc. Am.*, **93** (2003) 674.
[49] YE L., LAY T., KANAMORI H. and KOPER K. D., *Pure App. Geophys.*, **173** (2016) 321.

Production Queries for the Author

AUTHOR: Please check VERY CAREFULLY throughout
1) TEXT (Copy-editing corrections already inserted in the manuscript-to-proofs process)
2) FIGURES (if any): All writings and symbols. Thank you

1 "...collocated GPS stations...": OK or "...co-located GPS stations..."? Thanks

2 "...number of colocated GNNS": should it be "number of co-located GNNS..."? Thanks

3 "...of which many collocated GNSS...": OK or should it be "...of which many co-located GNSS..."?

4 Author please check caption to fig. 2: OK "collocated" or should it be "co-located"?

5 "...at the PSGCX collocated with...": OK or should it be "... at the PSGCX co-located with..."?

6 "In the two bottom panels of fig. 8...": Do you mean "In the two bottom panels of fig. 6..."?

7 "...at the top of fig. 8...": Do you mean "...at the top of fig. 6..."? Thanks

8 "In fig. 6...": Do you mean "In fig. 7..."

9 "...shown in fig. 9b. ...": Ok or should it be "...shown in fig. 9, central panel". ...?."

10 "...collocated...": OK or "...co-located..."

11 Ref. [17] not quoted in main text: Please quote it or delete it from final list. Thanks

12 Ref. [19] not quoted in main text: Please quote it or delete it from final list. Thanks

13 Ref. [21] not quoted in main text: Please quote it or delete it from final list. Thanks

14 Ref. [33] not quoted in main text: Please quote it or delete it from final list.

Thanks

15 Ref. [40] not quoted in main text: Please quote it or delete it from final list. Thanks

16 Ref. [41] please check "NN" as page number. Thanks

17 Ref. [42] not quoted in main text: Please quote it or delete it from final list. Thanks